GRIFFITH UNIVERSITY

Characterisation of trehalose-6-phosphate phosphatases from bacterial pathogens

Author

Kim, Jun-Hong, Kim, Ji-Won, Jo, Jiwon, Straub, Jan Hendrik, Cross, Megan, Hofmann, Andreas, Kim, Jeong-Sun

Published

2020

Journal Title

Biochimica et Biophysica Acta (BBA) - Proteins and Proteomics

Version

Accepted Manuscript (AM)

DOI

10.1016/j.bbapap.2020.140564

Rights statement

© 2020 Elsevier. Licensed under the Creative Commons Attribution-NonCommercial-NoDerivatives 4.0 International Licence (http://creativecommons.org/licenses/by-nc-nd/4.0/) which permits unrestricted, non-commercial use, distribution and reproduction in any medium, providing that the work is properly cited.

Downloaded from

http://hdl.handle.net/10072/399641

Griffith Research Online

https://research-repository.griffith.edu.au

1
Characterisation of trehalose-6-phosphate phosphatases from bacterial pathogens
2
3
4

5 Jun-Hong Kim[a,1], Ji-Won Kim[a,1], Jiwon Jo[a,1], Jan Hendrik Straub[b], Megan Cross[b], Andreas
6 Hofmann[b,c,*], and Jeong-Sun Kim[a,*]
9 [a]Department of Chemistry, Chonnam National University, Gwangju 61186, Republic of Korea
10 [b]Griffith Institute for Drug Discovery, Griffith University, Nathan, Queensland 4111, Australia
11 [c]Department of Veterinary Biosciences, Melbourne Veterinary School, The University of
12 Melbourne, Parkville, Victoria 3010, Australia
13
14
15 [1]These authors contributed equally
16
17
18 [*]Corresponding authors: jsunkim@chonnam.ac.kr
19 a.hofmann@griffith.edu.au

20
21
22
23
24

Abstract

The trehalose biosynthesis pathway has recently received attention for therapeutic intervention combating infectious diseases caused by bacteria, helminths or fungi. Trehalose-6-phosphate phosphatase (TPP) is a key enzyme of the most common trehalose biosynthesis pathway and a particularly attractive target owing to the toxicity of accumulated trehalose-6-phosphate in pathogens.

Here, we characterised TPP-like proteins from bacterial pathogens implicated in nosocomial infections in terms of their steady-state kinetics as well as pH- and metal-dependency of their enzymatic activity. Analysis of the steady-state kinetics of recombinantly expressed enzymes from *Acinetobacter baumannii*, *Corynebacterium diphtheriae* and *Pseudomonas stutzeri* yielded similar kinetic parameters as those of other reported bacterial TPPs. In contrast to nematode TPPs, the divalent metal ion appears to be bound only weakly in the active site of bacterial TPPs, allowing the exchange of the resident magnesium ion with other metal ions. Enzymatic activity comparable to the wild-type enzyme was observed for the TPP from *P. stutzeri* with manganese, cobalt and nickel. Analysis of the enzymatic activity of *S. maltophilia* TPP active site mutants provides evidence for the involvement of four canonical aspartate residues as well as a strictly conserved histidine residue of TPP-like proteins from bacteria in the enzyme mechanism. That histidine residue is a member of an interconnected network of five conserved residues in the active site of bacterial TPPs which likely constitute one or more functional units, directly or indirectly cooperating to enhance different aspects of the catalytic activity.

Keywords

Catalyis; Cooperativity; Enzyme activity; Halo-acid dehydrogenase; Multi-drug resistance; Protein structure-function

1. Introduction

Following the discovery of penicillin in 1928, it has become a given that infectious diseases are curable by using antibiotic chemotherapeutics. However, over the past 20 years the imminent threat of increasing antibiotic resistance in pathogens and the need for suitable counter-measures has been recognised [1]. Clearly, antimicrobial resistance not only adds to the cost of health care through longer and more complicated therapies, but indeed jeopardises treatment of common infectious diseases and renders more complex medical procedures undertakings to be of very high risk [2]. These developments are exacerbated by the emergence of highly resistant bacteria over the past decade, after the pharmaceutical industry essentially stopped development of new antibiotics [3].

For example, whereas diphtheria is effectively controlled by vaccination, large outbreaks are not uncommon in countries or situations with compromised health infrastructure. Diphtheria is caused by the Gram-positive bacterium *Corynebacterium diphtheriae* and is typically treated with penicillin or erythromycin, but the occurrence of partially or fully resistant isolates has been reported for more than a decade (reviewed in [4]).

Among the Gram-negative bacteria (including *Pseudomonas aeruginosa*, *P. stutzeri*, *Acinetobacter baumanii* and *Stenotrophomonas maltophilia*), many behave as opportunistic pathogens in humans and thus pose a threat in particular through nosocomial infection. *S. maltophilia*, for example, can be isolated from environmental sources (including water, soil and plants), as well as animals, and poses a particular risk due to possible cross-transmission in hospitals and health care institutions [5–7], where it becomes a substantial threat for immunocompromised patients and neonates [8,9]. Although *Stenotrophomonas* is not inherently virulent and not currently considered to be of epidemic danger [9,10], the prevalence of *S. maltophilia* infection in the general population has been steadily increasing from 0.8% in 1997 to 1.7% in 2012 [11]. Owing to intrinsic resistance to

73 several different classes of antibiotics as well as their distinct epidemiology, bacteria such as *S.*
74 *maltophilia* are considered important emerging pathogens [12,13]. Further reasons for concern are
75 the development of resistance during treatment [14] and the acquired resistance to co-trimaxole, a
76 commonly prescribed combination therapeutic.

77 Accordingly, there is an urgency to develop alternative therapies and to explore opportunities that
78 might lead to new antibiotics [15]. Scientific advances of the past two decades, and in particular the
79 growing body of data originating from the various 'omics disciplines, have enabled protein-based
80 drug discovery strategies whereby the relationship between the structure and function of enzymes
81 important for pathogen survival can be exploited [16]. A promising approach in this context builds
82 on the selection of pathogen proteins operating in biochemical pathways that are different from or
83 absent in the host organism. It is hoped that by targeting such enzymes one can develop new
84 antibiotics with minimized side-effects.

85 One target for novel antimicrobials is the enzyme trehalose-6-phosphate phosphatase (TPP; E.C.
86 number 3.1.3.12) [17], a conserved enzyme of the commonest of five known trehalose biosynthesis
87 pathways. This enzyme is found in many pathogens, including bacteria, nematodes and yeast, but
88 absent from mammalian hosts and catalyses the last step in the so-called OtsAB pathway of
89 trehalose synthesis from uridine diphosphate-glucose and glucose 6-phosphate [18]. Structurally,
90 TPPs are members of the superfamily of haloacid dehalogenase (HAD) phosphatases, characterised
91 by a core domain with the topology of a Rossmann fold and a so-called cap domain formed by a
92 contiguous amino acid sequence 'inserted' into the sequence of the core domain [19]. The active
93 site is located in the interface between the core and cap domains and features a magnesium ion
94 coordinated by conserved aspartate residues. Based on particular amino acid residues involved in
95 the enzymatic mechanism of HAD phosphatases, four motifs (I – IV) [19] have been defined (see
96 Supplementary Figure S1).

97 In consideration of the structural topologies of mono-enzyme TPPs from pathogenic organisms, we
98 previously suggested the classification of these enzymes into three topological groups, thereby
99 distinguishing bacterial, mycobacterial and nematode TPPs [20]. In order to provide and broaden
100 knowledge on the group of bacterial TPPs, we investigated a selection of TPP-like proteins from
101 highly infectious bacteria that appear to develop antibiotic resistance, namely *A. baumannii*
102 (abbreviated as *Abau*), *C. diphtheriae* biovor belfantii or *C. belfantii* sp. nov (*Cdip*), *P. stutzeri*
103 (*Pstu*) and *S. maltophilia* (*Smal*). We determined and compared the kinetic parameters of T6Pase
104 activity of the four purified recombinant enzymes, investigated the metal ion dependency for *Pstu*-
105 TPP and the involvement of conserved active side residues in the bacterial group of TPPs by
106 generating point mutations of *Smal*-TPP.

107

108 **2. Materials and Methods**

109 *2.1 Cloning, expression and purification of bacterial TPPs*

110 Genes coding for *Abau*-TPP (gb:CAP01961.1), *Cdip*-TPP (gb:VVH29859.1) and *Pstu*-TPP
111 (gb:TGY11003.1) were synthesised with codon optimisation for expression in *Escherichia coli* by
112 Cosmogenetech (Seoul, Korea) and cloned into the vector pLIC.B3 to yield N-terminal fusion
113 constructs containing a hexa-histidine tag, followed by a tobacco etch virus (TEV) protease
114 cleavage site. Additionally, Abau-TPP was also ligated into pLIC.B4, thus affording a hexa-
115 histidine-maltose binding protein tag. pLIC-B3 and pLIC-B4 vectors are modified versions of pET-
116 21a (Novagen, Madison, WI, USA). The codon-optimised expression construct of *Smal*-TPP has
117 been described earlier [21] and also featured an N-terminal hexa-histidine tag with an upstream
118 TEV protease cleavage site. Using the *Smal*-TPP wild-type construct as a template, single amino
119 acid mutations were introduced to yield five mutant proteins: D23N, D25N, H85F, D204N and

D208N.

For expression and purification protocols, please see the Supplementary Materials and Methods. All stages of protein purification were monitored by SDS-PAGE confirming the expected molecular masses for the target proteins (Supplementary Figure S3).

2.2 Phosphatase assay

Phosphatase activity of recombinant TPPs was assessed using the BIOMOL® Green reagent (Enzo Life Sciences, New York, NY, USA) and trehalose-6-phosphate (Sigma Aldrich, St. Louis, USA) as substrate. The detailed experimental protocol is described in the Supplementary Materials and Methods.

2.3 pH dependency of enzyme activity

The enzyme activity under varying pH conditions was assessed in endpoint assays with a reaction time of 30 min (*Abau*-TPP), 5 min (*Cdip*-TPP, *Pstu*-TPP and *Smal*-TPP); the incubation times were chosen based on preliminary results from initial phosphatase assays with each protein. Reactions were initiated by the addition of 200 µM substrate to a solution of enzyme (0.25–2.5 µM) in buffer containing 100 mM NaCl and either sodium malonate (pH 4), sodium citrate (pH 5), MES (pH 6), TRIS-HCl (pH 7, 8), BICINE (pH 9), or CAPS (pH 10). The final pH of each buffer solution was measured using a pH meter (Denver Instrument, Bohemia, USA; Thermo Scientific, Waltham, USA).

2.4 Steady-state enzyme kinetics

For the enzyme kinetics, the time-dependent product formation at room temperature was assessed to calculate the initial rates. Each recombinant enzyme was diluted into a buffer solution of 100 mM NaCl and 20 mM TRIS (pH 7.5) to achieve a final protein concentration of 30 µM (*Abau*-TPP) or 0.05 µM (*Cdip*-TPP, *Pstu*-TPP), respectively. Reactions in a total volume of 0.5 ml were started by adding substrate at a final concentration of 200 µM and stopped at various time points by quenching with BIOMOL® Green reagent. Initial rates were determined by fitting the time course data with a saturation curve and determining the slope at time $t = 0$; data analysis was done with SDAR (version 5.2) [22].

2.5 Endpoint assays to assess metal dependency and enzyme activity of mutants

To remove any resident magnesium ions, purified *Pstu*-TPP was dialysed against 100 mM NaCl, 1 mM EDTA and 20 mM TRIS (pH 7.5). To assess the effect of different divalent metal ions on the enzyme activity of *Pstu*-TPP, 1 µM enzyme was mixed with 10 mM metal chloride salt in assay buffer (100 mM NaCl, 20 mM TRIS, pH 7.5). For assessment of *Smal*-TPP mutants a final concentration 0.25 µM protein and 1 mM $MgCl_2$ in the assay buffer was used.

The relative phosphatase activity of *Pstu*-TPP in the presence of different metals or *Smal*-TPP mutants was determined using an endpoint that followed the same general protocol as above. Reactions were initiated by the addition of 100 µM (*Pstu*-TPP) or 200 µM (*Smal*-TPP) substrate and allowed to proceed for 5 min before quenching with the BIOMOL® Green reagent.

162 **3. Results and Discussion**

163 *3.1 Expression and purification*

164 The amino acid sequences of the four selected proteins possess all hallmark features expected for
165 genuine TPPs (Supplementary Figure S1) and share sequence identities between 27% and 41%
166 among each other (Supplementary Table S2). The synthetic genes encoding TPPs of *A. baumannii*,
167 *C. diphtheriae*, *P. stutzeri* and *S. maltophilia* were each ligated into an expression vector that
168 contained an N-terminal hexa-His-tag and a tobacco etch virus (TEV) protease cleavage site to
169 afford purification by affinity chromatography and removal of the fusion peptide. Whereas
170 recombinant *Smal*-TPP had been expressed and purified previously [21], recombinant TPP-like
171 proteins from *A. baumannii*, *C. diphtheriae*, *P. stutzeri* were produced here for the first time.
172 Expression of His-tagged *Abau*-TPP resulted in insoluble protein preparations, hence a fusion
173 construct with maltose-binding protein was generated. For all enzyme assays the purified
174 recombinant proteins after removal of the N-terminal fusion peptides were used, except for the
175 enzyme from *A. baumannii*. Due to solubility issues of this recombinant protein, the complete
176 fusion construct including the N-terminally fused maltose binding protein was used.

177

178 *3.2 pH dependency of enzyme activity*

179 As an initial characterisation of the enzyme activity of the four purified recombinant proteins, the
180 pH dependency of catalysed trehalose-6-phosphate hydrolysis was assessed. For *Cdip*-TPP, *Pstu*-
181 TPP and *Smal*-TPP the highest enzymatic activity was observed in the pH range 6.7 – 7.7 (Figure
182 1). The observed bell-shaped plot of enzyme activity versus pH is in agreement with an enzyme
183 mechanism involving two ionisable residues. From this analysis, the apparent pK_a values of the two
184 amino acid residues directly involved in the catalytic reaction can be estimated (Table 1). Owing to
185 the instability of purified recombinant *Abau*-TPP at pH values substantially different from pH 7, it
186 was not possible to analyse the pH dependency of enzymatic activity for this protein.

187 Since the pH dependence curve shows a rather sharp peak, the pK_a values of the two ionisable
188 residues involved in the catalytic reaction are less than one pH unit apart and probably do not titrate
189 independently; the estimated pK_a values have thus been termed apparent. Intriguingly, for bacterial
190 TPPs, the estimated apparent pK_{a2} values are in the range of 7.1–8.1 and therefore much higher than
191 the pK_a value of free aspartic acid. Whereas such discrepancies are frequently observed in enzymes
192 due to the particular environments within folded proteins [23,24], it is also possible that these
193 observed pK_a values reflect the involvement of more basic residues or indeed interconnected
194 functional units within the active site.

195

196 *3.3 Steady-state enzyme kinetics*

197 Owing to the exquisite substrate specificity of TPPs, the wild-type enzymes *Abau*-TPP, *Cdip*-TPP
198 and *Pstu*-TPP were subjected to a phosphatase kinetics endpoint assay using trehalose-6-phosphate
199 as substrate. The amount of released phosphate was determined by absorbance measurement at 645
200 nm, utilising a phosphate standard curve determined (Supplementary Figure S4). The enzyme
201 kinetics and steady parameters of *Smal*-TPP have been reported previously [21].

202 For all four bacterial TPPs, the steady-state kinetics can be fitted with a Michaelis-Menten model
203 (Figure 2), yielding K_M values between 0.76 and 3.0 mM and are thus in the same range as those
204 reported for other bacterial TPPs (see Table 2). For *Cdip*-, *Pstu*- and *Smal*-TPP, the k_{cat} values
205 ranging from 0.23 to 22 s^{-1} also compare well with the turnover numbers known for other bacterial
206 TPPs. However, *Abau*-TPP was observed as a very slow enzyme in the enzyme panel tested here,
207 exhibiting a k_{cat} of 0.004 s^{-1}. The low turnover number observed for this enzyme is most likely due

208 to the impaired stability of recombinant *Abau*-TPP that rendered the kinetics experiments spurious.

209

210 *3.4 Metal dependency of* Pstu-*TPP enzyme activity*

211 Catalytic hydrolysis of T6P by reported TPPs requires the presence of a magnesium ion coordinated
212 by two of the conserved aspartate residues in the active site. A survey of currently available
213 experimental structures of bacterial TPPs shows that these are usually the first aspartate residues of
214 the conserved HAD motifs I (DXDGT) and IV (DXXXD). However, in contrast to observations
215 with nematode and mycobacterial enzymes, only TPPs from the bacterial group have previously
216 been shown to be susceptible to inhibition by EDTA **[21,25]**, indicating that binding of the divalent
217 metal ion in bacterial TPPs is weaker than in those of the other two groups.

218 Using *Pstu*-TPP as a representative member of the bacterial group of TPPs in the present study, we
219 detected no release of free phosphate from T6P after treatment of *Pstu*-TPP with EDTA (Figure 3).
220 The catalytic activity of EDTA-treated *Pstu*-TPP could be restored when magnesium ions were
221 added into the reaction mixture. In further assays with EDTA-treated *Pstu*-TPP, we explored the
222 ability of a selection of other divalent metal ions to catalyse T6Pase activity. As seen in Figure 3,
223 phosphate hydrolysis of the T6P substrate was possible with Co^{2+}, Ni^{2+} and Mn^{2+}, but not with Ca^{2+},
224 Fe^{2+}, Zn^{2+} or Cd^{2+}.

225

226 *3.5 Enzyme activity of active site aspartate mutants of* Smal-*TPP*

227 A hallmark feature of the HAD superfamily are the four motifs I – IV of conserved amino acid
228 residues that are located in or close to the active site and involved in the catalytic mechanism [19].
229 As mentioned above, motifs I and IV provide four strictly conserved aspartate residues. In order to
230 validate the involvement of these residues in the enzymatic activity of bacterial TPPs, using *Smal*-
231 TPP as the representative protein in this instance. Single-site asparagine mutants were generated for
232 the four *Smal*-TPP residues 23, 25, 204 and 208, and their T6Pase activity was assessed.
233 Intriguingly, the catalytic activity was entirely suppressed for all four Asp→Asn mutants (Figure 4).
234 In comparison, a similar analysis of the aspartate residues of the nematodal *Brugia malayi* TPP
235 (residues 213, 215, 424, 428) yielded suppression of the catalytic activity only for the second
236 positions in each of the two motifs (i.e. residues 215, 428), whereas the mutants altering the first
237 positions (213 and 424) still showed near-wild type catalytic activity [20]. This latter result is in
238 agreement with the assumption that the first aspartate residues of both motifs coordinate the
239 divalent metal ion in the active site (which is still possible in the case Asp→Asn replacements), and
240 the second aspartate residues of both motifs are directly involved in substrate binding and/or
241 nucleophilic attacks (not possible if the carboxylic acid is changed to an amide). The different
242 observation made with the bacterial TPP in this current study is most likely due to the lower binding
243 affinity of the divalent metal ion already demonstrated in the previous section. The higher
244 susceptibility of bacterial TPPs to inhibition by EDTA as compared to nematodal TPPs and the
245 complete suppression of enzymatic activity in case of all four aspartate mutants indeed indicate
246 weak binding of the divalent metal ion by bacterial TPPs.

247

248 *3.6 Bacterial TPPs possess a conserved histidine residue required for T6Pase activity*

249 Upon close inspection of grouped amino acid sequence alignment of mono-enzyme TPPs [20], a
250 specific histidine residue (see the residue labelled ‘1’ in Supplementary Figure S1) of the bacterial
251 and mycobacterial groups becomes apparent that locates to the vicinity of the active site. In TPPs of
252 the nematodal group, this position is taken by a conserved tryptophan residue. In order to assess the
253 importance of this residue (position 85 in *Smal*-TPP) for the enzymatic activity, single site

mutagenesis was employed to replace this residue with phenylalanine in *Smal*-TPP. As can be seen in Figure 4, enzymatic T6Pase activity of the H85F mutant of *Smal*-TPP was completely suppressed. This suggests an involvement of this conserved residue in either substrate binding or indeed the catalytic mechanism perhaps as a supporting residue.

3.7 Evidence for an active site network in bacterial TPPs

The recently reported crystal structure of TPP from the bacterium *Salmonella typhimurium* in complex with the substrate mimic trehalose-6-sulphate (T6S) [26] provided an opportunity for structural appraisal of the conserved histidine residue (position 82 in *Styp*-TPP). Although situated close to the sulphate moiety of the ligand, the conserved histidine residue at position 85/82 is not engaged in direct interactions with the ligand (see Figure 5). However, the summary of relevant interactions in the active site of T6S-bound *Styp*-TPP as shown in Figure 5 clearly reveals a network of alternating acid/base groups constituted by conserved residues (His82, Glu167, Lys125, Glu123, His132) that line one side of the active site. Previous studies have pointed out the relevance surrounding residues in active sites of enzymes [27] and in particular the requirement of interconnectivity for functional catalytic units [28].

A mutagenesis study with *Brugia malayi* TPP reported a 12-fold, 400-fold and 100-fold decrease for single-point mutations at the sites of residues Glu167, Lys 125 and Glu123 (*Styp* numbering) [29]. Combined with the observed loss of catalytic activity for the mutant at position His82 (*Styp* numbering), there is mounting evidence for an interconnected functional unit in the active site of (myco-)bacterial TPPs.

4. Conclusions

The OtsAB trehalose biosynthesis pathway is of high interest for potential therapeutic intervention to combat infectious pathogens since this pathway is absent in mammalian organisms. Here, we characterised the recombinant proteins of four TPP-annotated genes from pathogenic bacteria, all of which possessed phosphatase activity on their native substrate trehalose-6-phosphate. Their steady-state kinetics parameters were comparable to those of other TPP-like proteins from bacteria.

In contrast to nematode and mycobacterial TPPs, members of the bacterial group of these enzymes exhibited a much weaker binding of the magnesium ion required for enzymatic catalysis, as evident from the high susceptibility to inhibition by EDTA and the possibility to replace the active site magnesium ion with particular divalent transition metal ions without compromising catalytic activity. The complete suppression of enzyme activity observed with active site aspartate mutants further indicates subtle specification of the otherwise shared enzymatic mechanism when comparing bacterial members with those of other groups of TPPs.

Within the present study, we also identified a strictly conserved histidine residue of bacterial and mycobacterial TPPs that is located in the vicinity of the active site and was crucial for enzyme activity, indicating that this residue is either involved in substrate binding or involved directly in the enzymatic reaction. In combining data from the present study with experimental results published previously, we believe that the network of five conserved residues in the active site of (myco-)bacterial TPPs constitutes one or more functional units that directly or indirectly cooperate to enhance different aspects of the catalytic activity. The detailed degree to which these units operate cooperatively or independently remains to be elucidated in a rigorous mutagenesis study, but recent research in this field [30] suggests that the active site in these enzymes has evolved to adopt a mechanism of partial cooperativity within the network of active site residues.

300 **Author contributions**

301 JHK, JWK, JJ and JHS performed the experiments. All authors analysed the data and wrote the
302 paper. MC, AH and JSK supervised the work. AH and JSK designed the study.

303

304 **Data availability**

305 All data supporting the findings of this study are available within this article and its supplementary
306 materials.

307

308 **Declaration of competing interests**

309 The authors declare that they have no known competing financial interests or personal relationships
310 that could have appeared to influence the work reported in this paper.

311

312 **Acknowledgements**

313 Research in the investigators' laboratories is funded by National Research Foundation of Korea
314 (grant No. NRF-2019R1I1A3A01061866 to JSK), the Australian Research Council (AH) and the
315 Rebecca L. Cooper Medical Research Foundation (AH). The Equity Trustees PhD Scholarship and
316 Australian Government Research Training Program Scholarship (MC), as well as support by a
317 DAAD RISE scholarship (JHS) are gratefully acknowledged.

318

319 **Appendix A. Supplementary data**

320 Supplementary data related to this article can be found online at
321 https://doi.org/10.1016/j.bbapap.2020.xxxxxx.

322

323 **References**

[1] D.M. Livermore, The need for new antibiotics, Clin. Microbiol. Infect. Off. Publ. Eur. Soc. Clin. Microbiol. Infect. Dis. 10 Suppl 4 (2004) 1–9. https://doi.org/10.1111/j.1465-0691.2004.1004.x.

[2] World Health Organisation, Antimicrobial resistance, Antimicrob. Resist. Factsheet. (2018). http://www.who.int/news-room/fact-sheets/detail/antimicrobial-resistance (accessed September 11, 2018).

[3] T. Braine, Race against time to develop new antibiotics, Bull. World Health Organ. 89 (2011) 88–89. https://doi.org/10.2471/BLT.11.030211.

[4] M. Hennart, L.G. Panunzi, C. Rodrigues, Q. Gaday, S.L. Baines, M. Barros-Pinkelnig, A. Carmi-Leroy, M. Dazas, A.-M. Wehenkel, X. Didelot, J. Toubiana, E. Badell, S. Brisse, Population genomics and antimicrobial resistance in Corynebacterium diphtheriae, BioRxiv. (2020) 2020.05.19.101030. https://doi.org/10.1101/2020.05.19.101030.

[5] D.G. de Viedma, M. Marín, E. Cercenado, R. Alonso, M. Rodríguez-Créixems, E. Bouza, Evidence of nosocomial *Stenotrophomonas maltophilia* cross-infection in a neonatology unit analyzed by three molecular typing methods, Infect. Control Hosp. Epidemiol. 20 (1999) 816–820. https://doi.org/10.1086/501590.

[6] H. Gulcan, C. Kuzucu, R. Durmaz, Nosocomial *Stenotrophomonas maltophilia* cross-infection: Three cases in newborns, Am. J. Infect. Control. 32 (2004) 365–368. https://doi.org/10.1016/j.ajic.2004.07.003.

[7] S. Valdezate, A. Vindel, L. Maiz, F. Baquero, H. Escobar, R. Canton, Persistence and variability of *Stenotrophomonas maltophilia* in cystic fibrosis patients, Madrid, 1991-1998,

Emerg. Infect. Dis. 7 (2001) 113–122. https://doi.org/10.3201/eid0701.700113.

[8] C.J. VanCouwenberghe, T.B. Farver, S.H. Cohen, Risk factors associated with isolation of *Stenotrophomonas* (*Xanthomonas*) *maltophilia* in clinical specimens, Infect. Control Hosp. Epidemiol. 18 (1997) 316–321.

[9] G. Samonis, D.E. Karageorgopoulos, S. Maraki, P. Levis, D. Dimopoulou, N.A. Spernovasilis, D.P. Kofteridis, M.E. Falagas, *Stenotrophomonas maltophilia* infections in a general hospital: Patient characteristics, antimicrobial susceptibility, and treatment outcome, PLOS ONE. 7 (2012) e37375. https://doi.org/10.1371/journal.pone.0037375.

[10] M.R.I. Höck, S. Swidsinski, B. Eberspächer, L. Schuster, R. Küchler, C. Grubel, U. Futh, L. Michalski, M. Kegel, B. Seefeld, E. Zill, R. Zuschneid, R. Schiller, K. Vogt, H. Stetzelberg, B. Hammer, B. Wilbrandt, K. Weist, J. Wagner, Bakterielle Erreger von Krankenhausinfektionen mit besonderen Resistenzen und Multiresistenzen, Bundesgesundheitsblatt - Gesundheitsforschung -Gesundheitsschutz. 47 (2004) 363–368. https://doi.org/10.1007/s00103-004-0812-9.

[11] Y.-T. Chang, C.-Y. Lin, Y.-H. Chen, P.-R. Hsueh, Update on infections caused by *Stenotrophomonas maltophilia* with particular attention to resistance mechanisms and therapeutic options, Front. Microbiol. 6 (2015) 893. https://doi.org/10.3389/fmicb.2015.00893.

[12] W.J. Looney, M. Narita, K. Mühlemann, *Stenotrophomonas maltophilia*: an emerging opportunist human pathogen, Lancet Infect. Dis. 9 (2009) 312–323. https://doi.org/10.1016/S1473-3099(09)70083-0.

[13] A. Safdar, K.V. Rolston, *Stenotrophomonas maltophilia*: changing spectrum of a serious bacterial pathogen in patients with cancer, Clin. Infect. Dis. 45 (2007) 1602–1609. https://doi.org/10.1086/522998.

[14] M.W. Garrison, D.E. Anderson, D.M. Campbell, K.C. Carroll, C.L. Malone, J.D. Anderson, R.J. Hollis, M.A. Pfaller, *Stenotrophomonas maltophilia*: emergence of multidrug-resistant strains during therapy and in an in vitro pharmacodynamic chamber model, Antimicrob. Agents Chemother. 40 (1996) 2859–2864.

[15] C.L. Ventola, The antibiotic resistance crisis: part 1: causes and threats, P T Peer-Rev. J. Formul. Manag. 40 (2015) 277–283.

[16] I.D. Kuntz, Structure-based strategies for drug design and discovery, Science. 257 (1992) 1078–1082. https://doi.org/10.1126/science.257.5073.1078.

[17] M. Cross, S. Rajan, S. Biberacher, S.-Y. Park, M.J. Coster, E. Długosz, J.-S. Kim, R.B. Gasser, A. Hofmann, Trehalose-6-phosphate phosphatase as a broad-spectrum therapeutic target against eukaryotic and prokaryotic pathogens, Emerg. Top. Life Sci. 1 (2017) 675–683. https://doi.org/10.1042/ETLS20170106.

[18] N. Avonce, A. Mendoza-Vargas, E. Morett, G. Iturriaga, Insights on the evolution of trehalose biosynthesis, BMC Evol. Biol. 6 (2006) 109. https://doi.org/10.1186/1471-2148-6-109.

[19] A.M. Burroughs, K.N. Allen, D. Dunaway-Mariano, L. Aravind, Evolutionary genomics of the HAD superfamily: Understanding the structural adaptations and catalytic diversity in a superfamily of phosphoesterases and allied enzymes, J. Mol. Biol. 361 (2006) 1003–1034. https://doi.org/10.1016/j.jmb.2006.06.049.

[20] M. Cross, R. Lepage, S. Rajan, S. Biberacher, N.D. Young, B.-N. Kim, M.J. Coster, R.B. Gasser, J.-S. Kim, A. Hofmann, Probing function and structure of trehalose-6-phosphate phosphatases from pathogenic organisms suggests distinct molecular groupings, FASEB J. 31 (2017) 920–926. https://doi.org/10.1096/fj.201601149R.

[21] M. Cross, S. Rajan, J. Chekaiban, J. Saunders, C. Hamilton, J.-S. Kim, M.J. Coster, R.B. Gasser, A. Hofmann, Enzyme characteristics of pathogen-specific trehalose-6-phosphate phosphatases, Sci. Rep. 7 (2017) 2015. https://doi.org/10.1038/s41598-017-02220-2.

[22] S. Weeratunga, N.-J. Hu, A. Simon, A. Hofmann, SDAR: a practical tool for graphical analysis of two-dimensional data, BMC Bioinformatics. 13 (2012) 201. https://doi.org/10.1186/1471-

2105-13-201.
[23] T.K. Harris, G.J. Turner, Structural basis of perturbed pKa values of catalytic groups in enzyme active sites, IUBMB Life. 53 (2002) 85–98. https://doi.org/10.1080/15216540211468.
[24] G.D. Nardo, M. Breitner, A. Bandino, D. Ghosh, G.K. Jennings, J.C. Hackett, G. Gilardi, Evidence for an elevated aspartate pKa in the active site of human aromatase, J. Biol. Chem. 290 (2015) 1186–1196. https://doi.org/10.1074/jbc.M114.595108.
[25] M. Cross, S. Biberacher, S.-Y. Park, S. Rajan, P. Korhonen, R.B. Gasser, J.-S. Kim, M.J. Coster, A. Hofmann, Trehalose 6-phosphate phosphatases of *Pseudomonas aeruginosa*, FASEB J. 32 (2018) 5470–5482. https://doi.org/10.1096/fj.201800500R.
[26] C. Harvey, K. O'Toole, C. Liu, P.S. Mariano, D. Dunaway-Mariano, K.N. Allen, Structural analysis of binding determinants of *Salmonella typhimurium* trehalose-6-phosphate phosphatase using ground-state complexes, Biochemistry (Mosc.). 59 (2020) 3247–3257. https://doi.org/10.1021/acs.biochem.0c00317.
[27] G.J. Narlikar, D. Herschlag, Direct demonstration of the catalytic role of binding interactions in an enzymatic reaction, Biochemistry (Mosc.). 37 (1998) 9902–9911. https://doi.org/10.1021/bi980495t.
[28] D.A. Kraut, K.S. Carroll, D. Herschlag, Challenges in enzyme mechanism and energetics, Annu. Rev. Biochem. 72 (2003) 517–571. https://doi.org/10.1146/annurev.biochem.72.121801.161617.
[29] J.D. Farelli, B.D. Galvin, Z. Li, C. Liu, M. Aono, M. Garland, O.E. Hallett, T.B. Causey, A. Ali-Reynolds, D.J. Saltzberg, C.K.S. Carlow, D. Dunaway-Mariano, K.N. Allen, Structure of the trehalose-6-phosphate phosphatase from *Brugia malayi* reveals key design principles for anthelmintic drugs, PLoS Pathog. 10 (2014) e1004245. https://doi.org/10.1371/journal.ppat.1004245.
[30] F. Sunden, A. Peck, J. Salzman, S. Ressl, D. Herschlag, Extensive site-directed mutagenesis reveals interconnected functional units in the alkaline phosphatase active site, ELife. 4 (2015) e06181. https://doi.org/10.7554/eLife.06181.
[31] S. Suthisawat, L.J. Gourlay, M. Bolognesi, U. Boonyuen, M. Vanaporn, Functional and structural analysis of trehalose-6-phosphate phosphatase from *Burkholderia pseudomallei*: Insights into the catalytic mechanism, Biochem. Biophys. Res. Commun. 523 (2020) 979–984. https://doi.org/10.1016/j.bbrc.2019.12.088.
[32] H.S. Seo, Y.J. Koo, J.Y. Lim, J.T. Song, C.H. Kim, J.K. Kim, J.S. Lee, Y.D. Choi, Characterization of a bifunctional enzyme fusion of trehalose-6-phosphate synthetase and trehalose-6-phosphate phosphatase of *Escherichia coli*, Appl. Environ. Microbiol. 66 (2000) 2484–2490. https://doi.org/10.1128/aem.66.6.2484-2490.2000.
[33] C. Liu, D. Dunaway-Mariano, P.S. Mariano, Rational design of first generation inhibitors for trehalose 6-phosphate phosphatases, Tetrahedron. 73 (2017) 1324–1330. https://doi.org/10.1016/j.tet.2017.01.041.
[34] R Core Team, R: A language and environment for statistical computing, R Foundation for Statistical Computing, Vienna, Austria, 2017. https://www.R-project.org/.
[35] A. Hofmann, M. Cross, M.A. Karow, J.H. Straub, C.S. Clemen, L. Eichinger, A convenient tool for bivariate data analysis and bar graph plotting with R, Biochem. Mol. Biol. Educ. 47 (2019) 207–210. https://doi.org/10.1002/bmb.21205.
324

325 **Tables**

326

327 **Table 1: Estimated apparent pK_a values of the residues involved in the catalytic reaction**

328

Enzyme	pK_{a1}^{app}	pK_{a2}^{app}	Reference
Cdip-TPP	6.3	7.2	this study
Paer-chTPP	6.2	7.1	[25]
Paer-ecTPP	6.5	7.3	[25]
Pstu-TPP	7.4	8.1	this study
Smal-TPP	7.4	8.1	this study

329

330

331

332 **Table 2: Comparison of steady-state kinetics parameters of bacterial TPPs**

333 Values in parentheses indicate the [a]standard error, [b]standard deviation or [c]unspecified error.

334

Enzyme	K_M (mM)	k_{cat} (s^{-1})	k_{cat} / K_M (M^{-1} s^{-1})	Reference
Abau-TPP	0.76 (0.04[a])	0.004 (0.002[a])	5.7	this study
Bpse-TPP	0.17	2.6	15×10^3	[31]
Cdip-TPP	3.0 (0.83[a])	5.2 (0.82[a])	1.7×10^3	this study
Ecol-TPP	2.5 (0.1[b])	14 (0.6[b])	5.7×10^3	[32]
Paer-chTPP	3.2	0.06	0.02×10^3	[25]
Paer-ecTPP	4.2	0.06	0.01×10^3	[25]
Pstu-TPP	0.91 (0.02[a])	22 (2.6[a])	24×10^3	this study
Sboy-TPP	0.69 (0.07[c])	16 (1[c])	23×10^3	[33]
Smal-TPP	2.0	0.23	0.11×10^3	[21]
Styp-TPP	0.31 (0.04[c])	6.2 (0.3[c])	20×10^3	[33]

335

336

Figure legends

Figure 1: pH dependency of the catalytic activity of three bacterial TPPs.
Individual data points for *Cdip*-TPP (red; A_{645}), *Pstu*-TPP (green; A_{645}) and *Smal*-TPP (blue; A_{620}) represent the mean value of at least three independent experiments and error bars indicate one standard deviation. Data were fitted with a Gaussian function (solid lines) to determine the value of the optimum pH. Analysis and figure preparation was done with SDAR (version 5.2) [22].

Figure 2: Steady-state kinetics of three bacterial TPPs
Data points show the initial rate of T6P hydrolysis catalysed by *Abau*-TPP (30 µM), *Cdip*-TPP (0.05 µM) and *Pstu*-TPP (0.05 µM). Time-dependent product formation was measured at varying initial substrate concentrations. Different initial substrate concentrations and the initial rates obtained from the slope of the fitted curves at time $t = 0$. The discrete data points represent the mean value of at least three independent experiments, and error bars indicate one standard deviation. The solid lines represent fits of the Michaelis-Menten equation; for numerical results see Table 2.

Figure 3: Metal dependency of *Pstu*-TPP enzyme activity.
The bar graph shows the relative catalytic T6P phosphatase activity of purified recombinant *Pstu*-TPP, after dialysis against 1 mM EDTA and supplemented with 10 mM of divalent metal ions supplied as chloride salts. Endpoint assays using 1 µM enzyme and 100 µM substrate were used. The individual bars show the mean activity of three replicates, normalised with respect to the activity of the purified recombinant enzyme (left-most bar). Error bars indicate the standard deviation. Analysis and figure preparation was done with R (version 3.4.3) [34].

Figure 4: Enzymatic activity of *Smal*-TPP wild-type and mutants.
The bar graph shows the relative catalytic T6P phosphatase activity of wild-type and mutant *Smal*-TPP proteins as determined in endpoint assays using 2.5 µM enzyme and 100 µM substrate. The individual bars show the mean activity of three replicates, normalised with respect to the activity of the wild-type (WT) enzyme. Error bars indicate the standard error; significance was assessed by a two-tailed *t*-test with '***' indicating $p < 0.001$. Data analysis and figure generation was done with R (version 3.4.3) [34] and jBar (version 0.6) [35] for calculation of means and standard deviations, background correction, normalisation and significance evaluation by a two-sided *t*-test.

Figure 5: A network of conserved residues lining the active site suggests interconnected functional units.
Summary of relevant interactions between active site residues of *S. typhimurium* TPP and the substrate-mimicking ligand trehalose-6-sulphate based on the reported crystal structure (PDB ID 6upc). Values indicate the atomic distance in Å. The residues forming the alternating acid/base network are labelled '1'–'5' in Supplementary Figure S1. Interactions in the grey-shaded area are included for an overview only; some interactions of the sulphate group have been omitted for clarity.

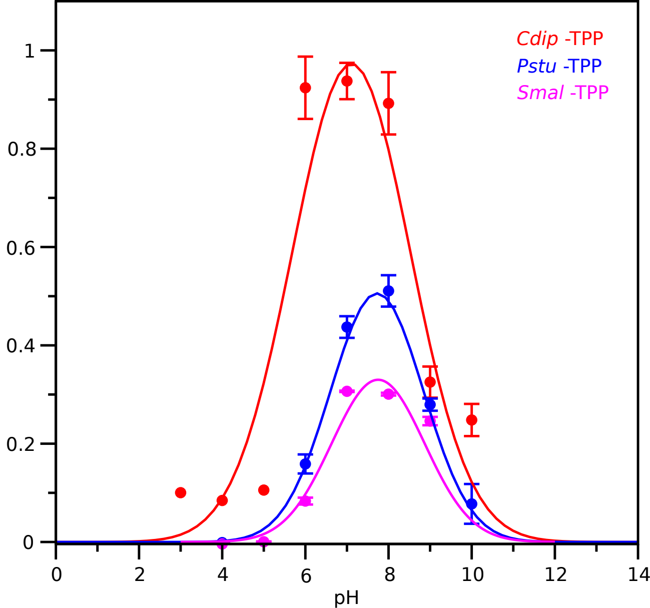
Cdip -TPP
Pstu -TPP
Smal -TPP
Absorbance at 620 nm or 645 nm
pH
0
0.2
0.4
0.6
0.8
1
0
2
4
6
8
10
12
14

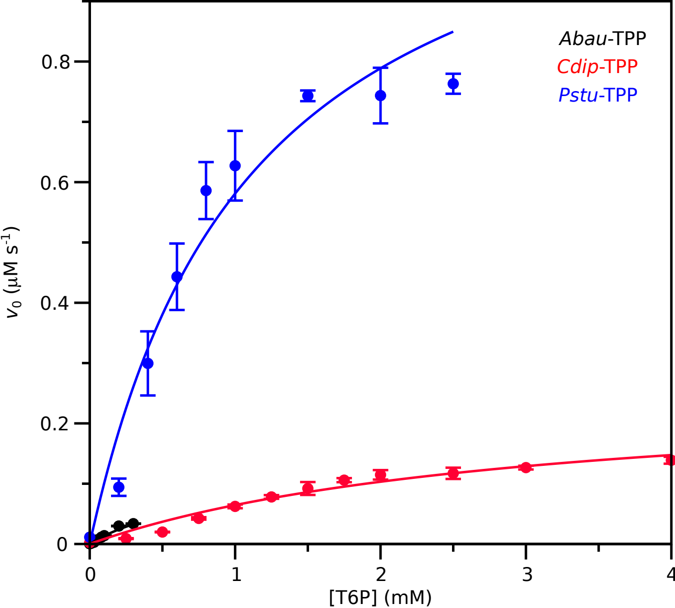
Abau-TPP
Cdip-TPP
Pstu-TPP
v_0 (μM s^{-1})
[T6P] (mM)
0
0.2
0.4
0.6
0.8
0
1
2
3
4

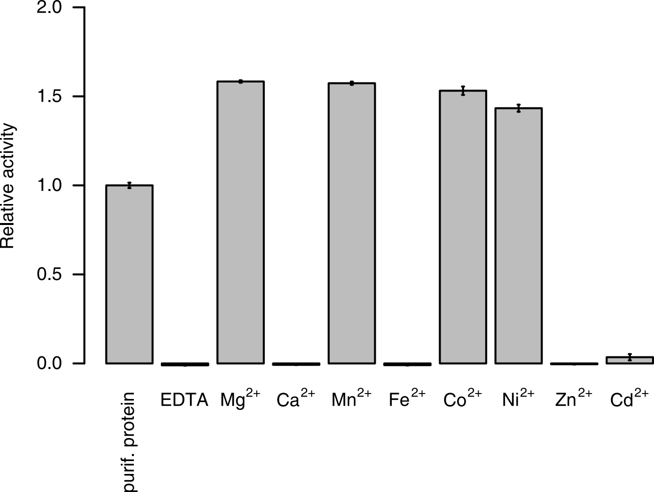

2.0
1.5
1.0
0.5
0.0
Relative activity
purif. protein
EDTA
Mg2+
Ca2+
Mn2+
Fe2+
Co2+
Ni2+
Zn2+
Cd2+

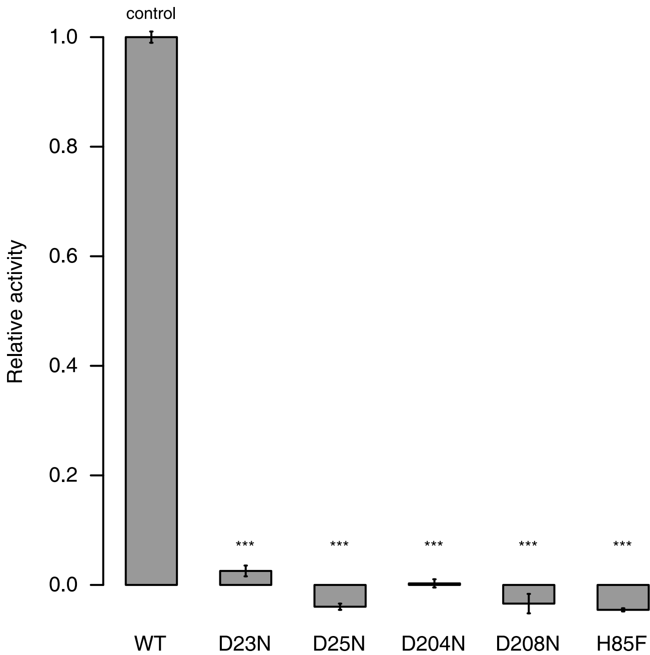
control
1.0
0.8
0.6
0.4
0.2
0.0
Relative activity
***
***
***
***
***
WT
D23N
D25N
D204N
D208N
H85F

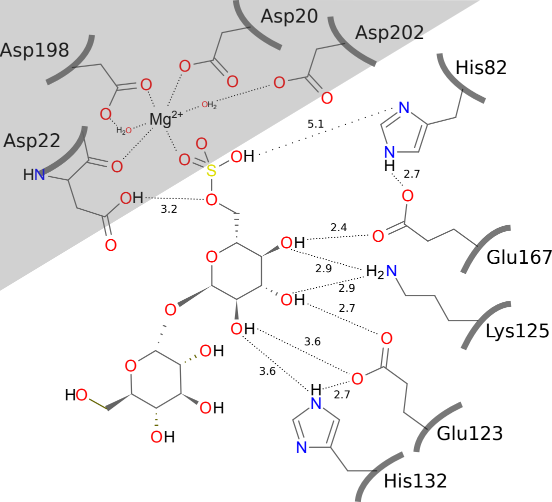
Asp198
Asp20
Asp202
His82
Asp22
Mg2+
5.1
2.7
3.2
2.4
Glu167
2.9
2.9
2.7
Lys125
3.6
3.6
2.7
Glu123
His132